Modelling 2D Coastal Flooding at Fine-scale Over Vulnerable Lowlands using Satellite-derived Topobathymetry, Hydrodynamic and Overflow Simulations

Antoine Collin, Coraline Calle, Dorothée James, Stéphane Costa, Olivier Maquaire, Robert Davidson, Antonio Trigo-Teixeira

Modelling 2D Coastal Flooding at Fine-scale Over Vulnerable Lowlands using Satellite-derived Topobathymetry, Hydrodynamic and Overflow Simulations

Antoine Collin[†*], Coraline Calle[†], Dorothée James[†], Stéphane Costa[‡], Olivier Maquaire[‡], Robert Davidson[‡], and Antonio Trigo-Teixeira[§]

[†]EPHE, PSL Université Paris
CNRS LETG
Dinard, France

[‡]Normandie Univ
UNICAEN
CNRS LETG Caen, France

[§]CERIS, Instituto Superior Tecnico
Lisbon University
Lisbon, Portugal

Flooding simulation across shallow waters and lowlands has been successful for the diagnosis and prognosis of the submerged land areas during extreme sea water levels. However this method is traditionally implemented to linear transects (1D) of discretely-measured topobathymetry or medium-to-coarse-grained 2D modelling. This research aims at mapping the coastal flooding risk at very high spatial resolution (1 m) by simulating hazardous cyclonic waves on exposed lands and vulnerable buildings using a combination of satellite-derived topobathymetry, wave transformation and overflow modelling. Applied to the Rangiroa Atoll (French Polynesia), the topobathymetry mapping resulted from the merging of the topography derived from the Pleiades-1 stereo-photogrammetry (R^2=0.84) and bathymetry retrieved from the Pleiades-1 radiative transfer modelling (R^2=0.71). Associated with the exposure index, the wave simulation of the 1983-cyclone Orama-Nisha produced hazardous heights of 1.78 m before the swash area, what enabled the lowlands' submersion to be mapped. Focused on churches and houses' vulnerability, the standardized flooding risk has been mapped at 1 m, accurately informing the near-future planning for this atoll area.

INTRODUCTION

Worldwide lowlands, defined by the coastal land part below 10 m altitude (Lichter *et al.*, 2011), constitute 1.74% of total land areas but host 10.25% of total population (Neumann *et al.*, 2015). The human exposure is forecast to grow at the same rate of the on-going coastward migration for next decades (Neumann *et al.*, 2015). Developing countries in Africa and Asia are and will be the most exposed population to coastal hazards and flooding risks (Neumann *et al.*, 2015).

The risk, resulting from the combination of hazards, exposure, sensitivity and adaptive capacity (Kron, 2002), could be alleviated, along the coastal fringe, by the nature-based adaptation to sea-level rise, enabling water energy to be absorbed (rather than reflected) and water level to be kept up and even outpaced (Cheong *et al.*, 2013). Tropical mangroves and coral reefs are now recognized to offer an effective coastal protection by breaking and damping ocean waves (Sierra-Correa and Kintz, 2015).

Since the current and future most exposed coastal population (Africa and Asia) is provided with substantial natural barriers, due to the tropical weather favoring plant growth, the nature-based adaptation has to be confidently integrated into local strategies implemented for coping with the sea-level rise. However, those risky zones, predominantly poor, from an economic point of view, cannot be finely mapped. Contrary to developed countries benefiting from survey technologies of both land and water elevations, such as the topobathymetric LiDAR (Collin *et al.*, 2018a), exposed zones of developing countries can essentially rely on open-source or low-cost data (Collin, Nadaoka, and Nakamura, 2014).

The potential coastal hazards are shaped by the wave height and period, which directly interact with the bathymetric patterns. Freely-available bathymetric data are provided with 15 arc-second pixel size (around 450 m at the equator) thanks to the General Bathymetric Chart of the Oceans (GEBCO) 2019, in which "the accuracy and completeness cannot be guaranteed", what hinders the numerical modelling of hazard integrating complex wave, tide, and seabed features. About the exposure, the global population can be complimentarily derived from the Gridded Population of the World (GPW) version 4, but at a spatial resolution of 30 arc-

*Corresponding author: antoine.collin@ephe.psl.eu

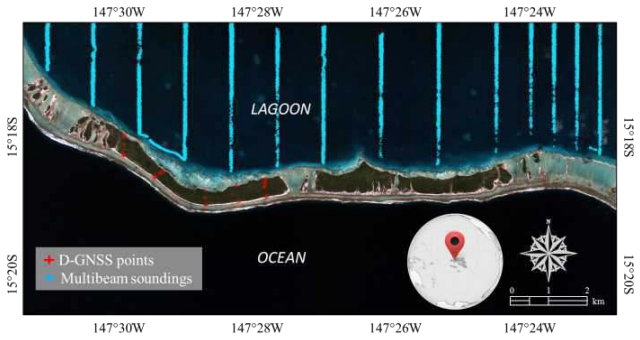

Figure 1. Natural-colored Pleiades-1 imagery of the study area of Otepipi (southern Rangiroa atoll, Tuamotu Archipelago) in French Polynesia. Red and blue crosses represent land (D-GNSS) and water (multibeam echosounder) calibration/validation points.

seconds (900 m at the equator). The topography could be computed based on worldwide digital elevation models (DEMs), such as Shuttle Radar Topography Mission (SRTM) level 1 from NASA, or Global DEM (DGEM) version 2 from joint US NASA and Japan METI, both at 1 arc-second spatial resolution (approximately 30 m at the equator). Both open-source datasets provide vertical information with an accuracy of 7 and 8 m (Elkhrachy, 2017), respectively, what impairs the rigorous delineation of lowlands. Regarding the nature-based adaptation, coastal barriers, such as saltmarshes and mangroves, can be captured at 30 m pixel size using high resolution satellite imagery (McOwen *et al.*, 2017; Sanderman *et al.*, 2018, respectively).

This work aims to create the first mapping of the flooding risk at very high resolution (VHR) based on satellite imagery and numerical modelling, so as to be used in remote or emerging countries. A Pleiades-1 stereo-imagery will be calibrated to get the VHR topobathymetry on which cyclone-driven hazardous waves will be simulated, enabling the exposure and vulnerability to be accounted for the risk mapping. As highly exposed, Rangiroa atoll will be the case study (Figure 1).

METHODS

Following the description of the study site, data collection and processing will be detailed as the satellite-derived topobathymetry and risk spatial modelling.

Rangiroa Atoll

Rangiroa (15°08'S, 147°36'W) is the second largest atoll in the world (oriented northwest-southeast, 80 km long and 32 km wide), which consists in 1446 km^2 of lagoon and 79 km^2 of land. Whilst the lagoon bottoms at 35 m deep (Kumar *et al.*, 2013), the terrestrial part (around 200 km long and 300 m wide maximum) is composed of 418 reef islands, and host 2 709 inhabitants over two islands (census 2017). Due to its large extent, Rangiroa atoll will be focused on the southeastern area, Otepipi, hosting 39 people, for this pilot study.

Satellite Imagery and By-Products

Spaceborne Pleiades-1 collected two imageries, in the form of a stereopair, on May, 31 2018 at 20h12'10" and 20h12'50" (UTC), respectively. This sensor can capture four multispectral

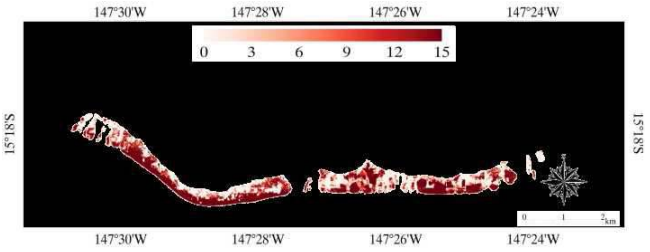

Figure 2. Digital Elevation Model (1 m) derived from the Pleiades-1 panchromatic stereopair.

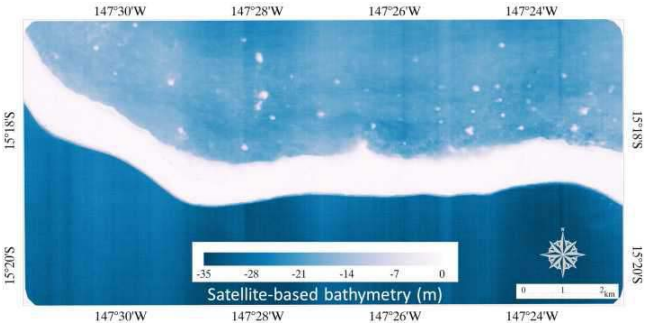

Figure 3. Digital Depth Model (1 m) derived from the Pleiades-1 pansharpened multispectral imagery.

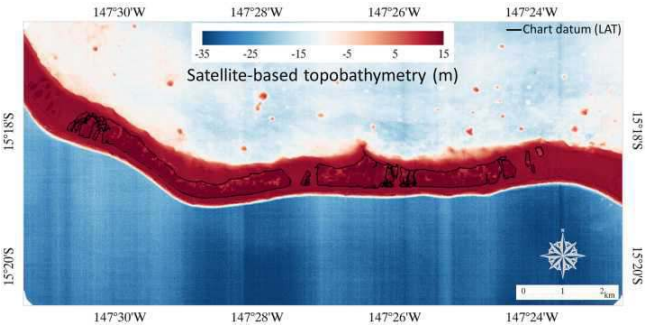

Figure 4. Digital Topobathymetric Model (1 m) derived from the Pleiades-1 datasets.

wavebands (blue: 430-550, green: 490-610, red: 600-720, near-infrared: 750-950 nm) at 2 m, and one panchromatic band (480-830 nm) at 0.5 m pixel size. Georeferenced into the datum RGPF, imageries were distinctly proceeded according to their topography and bathymetry fate.

Topography has been derived from the panchromatic stereopair, that were used for 3D point cloud generation from the semi-global matching algorithm (Gherke *et al.*, 2010), then digital surface model (DSM) and digital elevation model (DEM, Figure 2). The matching algorithm searches for the pairwise pixels of both imageries by simplifying the 2D epipolar dataset into 1D, based on rationale polynomial coefficients (RPCs). Resulting point cloud enabled to generate a DEM (projection UTM 6 South) at 1

m spatial resolution by interpolating local low elevation values, referenced to the chart datum (minimum water level during the lowest astronomical tide). A series of 51 D-GNSS measurements (Trimble R8S), surveyed and benchmarked in May 2018, allowed us to calibrate and validate the DEM with a satisfactory agreement (R^2=0.84, RMSE=0.9 m).

Bathymetry has been created using the multispectral imagery provided with the lowest incidence angle, pansharpened at 0.5 m and corrected for the geometry using RPCs (UTM 6 South). Following preliminary tests, no radiometric correction has been applied due to the best results with the digital number (DN). Resampled at 1 m pixel size, the bathymetry Z has been solved thanks to the ratio transform (Stumpf *et al.*, 2003), assuming that visible light absorption by water covariates with waveband:

$$Z = a_1 \left(\frac{\ln(R_w(\lambda_i) - R_\infty(\lambda_i)}{\ln(R_w(\lambda_j) - R_\infty(\lambda_j)} \right) - a_0 \quad (1)$$

where a_0 is the constant for a depth of 0 m, a_1 is the computed slope scaling the ratio to actual bathymetry, R_w is the DN related to the waveband λ_i, and R_∞ is the DN above optically deep water. An array of 1 584 multibeam echosounder soundings (R2Sonic 2024), collected between August and December 2011, calibrated and validated the digital depth model (DDM, Figure 3): R^2=0.71, RMSE=1.64 m.

Given the common zero between DEM and DDM, a VHR (1 m) topobathymetric model was implemented so as to support the flooding mapping (Figure 4).

Risk Mapping

The risk is the complex intersection of three components:

$$R = E \bigcap H \bigcap V \quad (2)$$

where, R is the flooding risk, E the exposure of the land area, H the wave-driven hazard from sea to land, and V the vulnerability of the built area.

The exposure stemmed from the joint information of shoreline distance and altitude. Supported by the natural-colored satellite imagery, the shoreline has been identified by the vegetation foot (Collin *et al.*, 2018b), enabling the creation of a 100-m landward buffer zone. Based on the satellite topography, the spatially-incremented buffer was further characterized by the pixel altitude. The resulting dataset was normally standardized.

The studied hazard was implemented in a VHR numerical modelling, so as to replay the hydrodynamic fate of the 3-category tropical cyclone Orama-Nisha in February 1983. Featured with sustained wind-speeds of 185 km.h^{-1}, a previous hydrodynamic and spectral modelling work computed that the cyclone generated wave height, period and direction of 4.9 m, 11 sec, and SW-NE, respectively (Damlamian and Kruger, 2013). The VHR behavior of wave heights' across the satellite bathymetry was predicted using a two-dimensional finite element wave transformation model combining diffraction, refraction, reflection, dissipation, breaking and dispersion phenomena (CGWAVE, Demirbilek and Panchang, 1998).

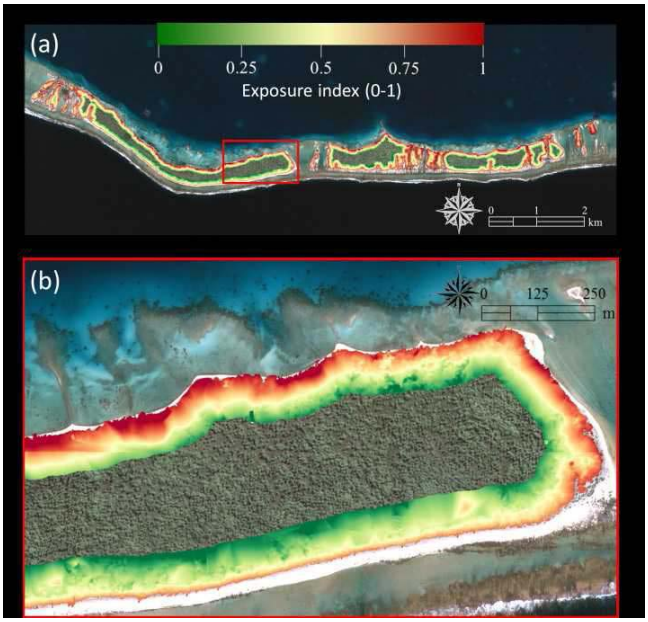

Figure 5. Exposure index (0-1) draped over the natural-colored Pleiades-1 imagery (a). Enlargement on the "future village" location in which the subtle exposure variations are made visible (b).

The vulnerability is composed of the sensitivity ratioed by the adaptive capacity, which is, here, embodied by the natural buffer of coral reefs. When healthy, the reefs dissipates wave energy by exerting a drag force on the body of water (Harris *et al.*, 2018). This nature-based adaptation is therefore included into the hazard simulation. Due to the reef protection ensured against the southern storm-driven swell, the studied sector, currently few populated, is planned to welcome a "future village" according to the local urbanism service. As a pilot project, the location and dimension of the planned buildings and infrastructures are not yet available, that is why the 28 existing buildings (26 copra houses and two churches) constituted the sensitivity component, with constant height values of 2.4 and 5 m, respectively (Worliczek, 2013).

RESULTS

Based on satellited-derived topobathymetry, the exposure index will be mapped, followed by the wave-driven hazardous flooding and building-based risk.

Mapping the Exposure to Coastal Flooding

The exposure index, as joint information of the 100-m buffer zone and satellite-based altitude, showed the highly exposed areas (in red in Figure 5), consistently oultined along transverse parts of small islets and over lagoonal shores (not facing ocean).

Mapping the Wave Hazard using Simulation

The simulated ocean intermediate waves, derived from the tropical cyclone Orama-Nisha, were strongly attenuated by the reef crest, falling from 5 to 2 m significant heights for the shallow-water (reef platform) waves (Figure 6). The mean height of the breakers attained 1.78 m.

The significant height of the hazardous breakers enabled the lowlands' swash area to be mapped as a function of their altitude,

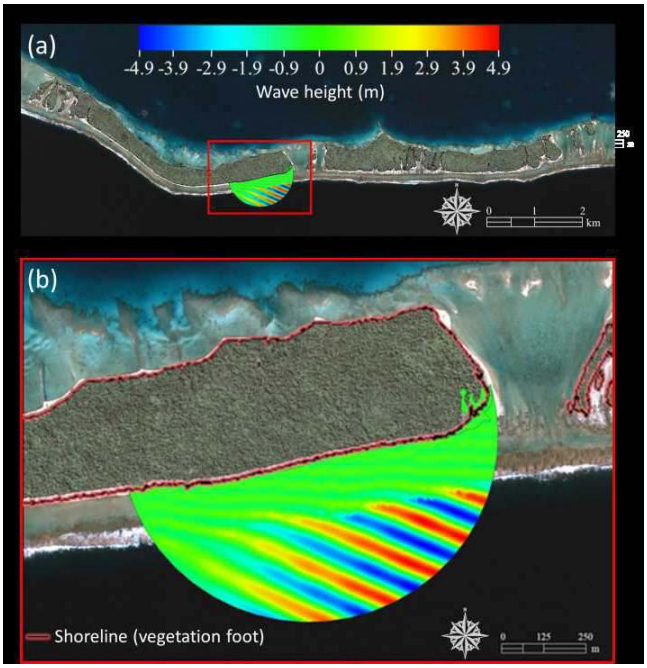

Figure 6. Wave height simulation of the 3-category tropical cyclone Orama-Nisha draped over the natural-colored Pleiades-1 imagery (a). Enlargement on the "future village" location in which the hazardous waves are made visible (b).

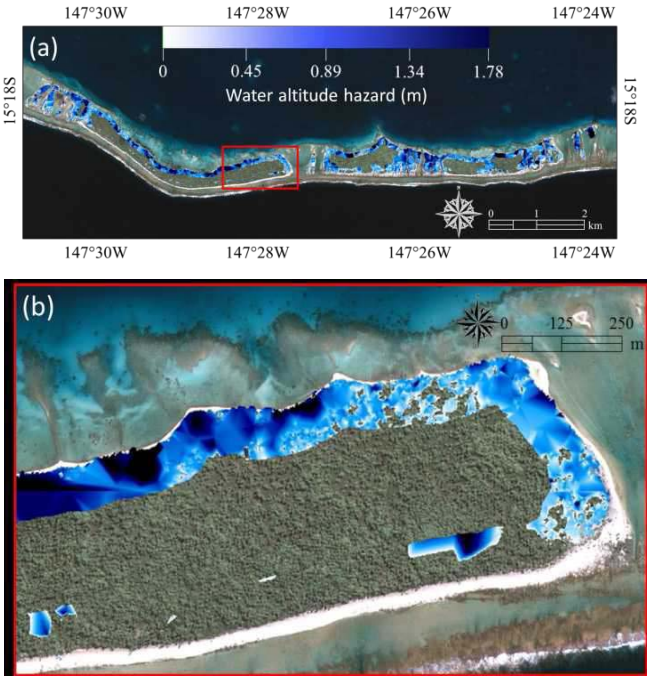

Figure 7. Water altitude hazard draped over the natural-colored Pleiades-1 imagery (a). Enlargement on the "future village" location in which the water altitude is made visible (b).

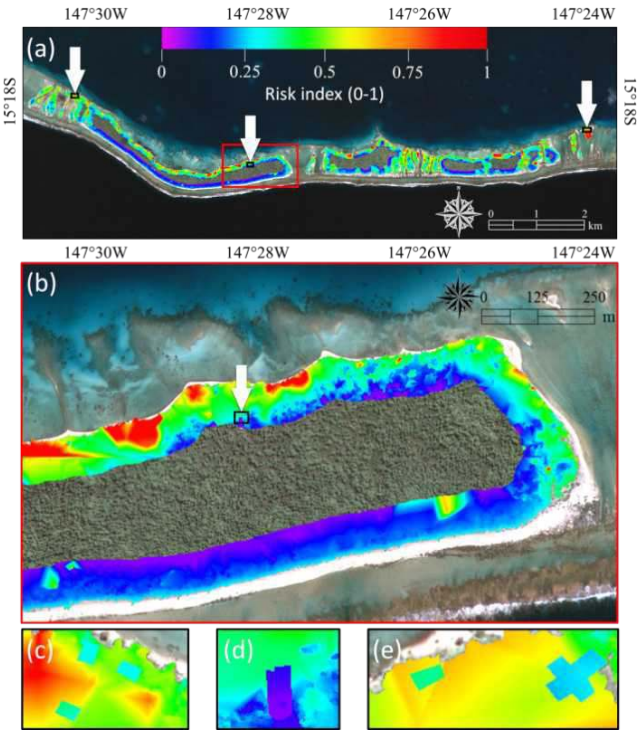

Figure 8. Risk index (0-1) draped over the natural-colored Pleiades-1 imagery (a). Enlargement on the "future village" location in which the subtle risk variations are made visible (b). Enlargement on three copra houses, located below the westernmost white arrow (c). Enlargement on the church of the "future village", located below the central white arrow (d). Enlargement on one copra house and the second church, located below the easternmost white arrow (d).

derived from the satellite topography (Figure 7). In addition to transverse parts and lagoonal shores, submerged areas were punctually found behind the coralligeneous dune.

Mapping the Risk of the Coastal Flooding

The risk index, as the intersection of the exposure and hazard, indicated both the general land use land cover and specific built areas subject to flooding (Figure 8). Since lagoonal shores appeared submerged, westernmost and easternmost houses (Figure 8c and 8e) were more at risk than the central church (Figure 8d).

DISCUSSION

The satellite-derived topobathymetry has a great potential to be transferable to worldwide coastal areas where the water clarity ranges from high to medium (Collin, Etienne, and Feunteun, 2017). Pleiades-1 topography was here much more accurate (RMSE=0.9 m) than this of Moorea (Collin *et al.*, 2018a, RMSE=7.49 m), what could be explained by the contribution of the calibration measurements. Contrariwise, Pleiades-1 bathymetry was twice less accurate here (RMSE=1.64 m) than this of Moorea (RMSE=0.88), what might result from the absence of nearshore calibration soundings.

The simuation of the wave propagation across the nearshore highlighted the strong role of the coral reef crest in hazard

attenuation. By simulating the cyclone-driven waves with the predicted sea-level heights, the coastal protection ensured by coral reefs will be quantified, so as to include the nature-based solutions into the climate change adaptation local policy.

The sensitivity of the buildings were estimated as constant height depending on their category (copra house or church). This risk component could be improved by using continuous measurements derived from a stereopair of the highest civilian spatial resolution WorldView-3 (0.3 m).

CONCLUSIONS

The VHR mapping of the marine flooding risk has been successfully implemented thanks to a combination of satellite-derived topobathymetry, nearshore wave propagation and overflow simulation. Pleiades-1 satellite-derived topography and bathymetry reached satisfactory agreements with ground-truth (R^2=0.84 and R^2=0.71, respectively). The exposure index resulted from the association of the 100m-buffer with altitude, both derived from the topobathymetry. The waves produced by the 1983-cyclone Orama-Nisha were simulated, providing 1.78m-height before the swash area, what enabled the lowlands' submersion to be mapped. Focused on churches and houses' vulnerability, the flooding risk could have been mapped at 1 m.

ACKNOWLEDGMENTS

This research was supported by the STORISK project (ANR-15-CE03-0003) funded by the National Agency for Research of France (ANR). Satellite imagery was acquired through ©CNES (2018), Airbus DS Distribution, all rights reserved.

LITERATURE CITED

Cheong, S.M.; Silliman, B.; Wong, P.P.; Van Wesenbeeck, B.; … and Guannel, G., 2013. Coastal adaptation with ecological engineering. *Nature climate change*, 3(9), 787.

Collin, A.; Duvat, V.; Pillet, V.; Salvat, B., and James, D., 2018b. Understanding the interactions between shoreline changes and reef outer slope morphometry on Takapoto Atoll (French Polynesia). *Journal of Coastal Research*, SI85, 496–500.

Collin, A.; Etienne, S., and Feunteun, E., 2017. VHR coastal bathymetry using WorldView-3: colour versus learner. *Remote Sensing Letters*, 8(11), 1072-1081.

Collin, A.; Hench, J.L.; Pastol, Y.; Planes, S.; ... and Troyer, M., 2018a. High resolution topobathymetry using a Pleiades-1 triplet: Moorea Island in 3D. *Remote sensing of environment*, 208, 109-119.

Collin, A.; Nadaoka, K., and Nakamura, T., 2014. Mapping VHR water depth, seabed and land cover using Google Earth data. *ISPRS International Journal of Geo-Information*, 3(4), 1157-1179.

Damlamian, H. and Kruger, J., 2013. Modèle bidimensionnel couplé de Rangiroa - Cyclone tropical Orama-Nisha (1983). Secretariat of the Pacific Community - Applied Geoscience and Technology Division, Suva, Fidji.

Demirbilek, Z. and Panchang, V., 1998. CGWAVE: A coastal surface water wave model of the mild slope equation (No. TR-CHL-98-26). Army Engineer Waterways Experiment Station Vicksburg MS.

Elkhrachy, I., 2017. Vertical accuracy assessment for SRTM and ASTER Digital Elevation Models: A case study of Najran city, Saudi Arabia. *Ain Shams Engineering Journal*, 9(4), 1807-1817.

Gehrke, S.; Morin, K.; Downey, M.; Boehrer, N., and Fuchs, T., 2010. Semi-global matching: An alternative to LIDAR for DSM generation. In *Proceedings of the 2010 Canadian Geomatics Conference and Symposium of Commission I*, 2(6).

Harris, D.L.; Rovere, A.; Casella, E.; Power, H.; ... and Parravicini, V., 2018. Coral reef structural complexity provides important coastal protection from waves under rising sea levels. *Science advances*, 4(2), eaao4350.

Kron, W., 2002. Keynote lecture: Flood risk = hazard× exposure× vulnerability. *Flood defence*, 82-97.

Kumar, S.; Kruger, J.; Begg, Z.; Handerson, E., and Alvis, M., 2013. SPC Applied Geoscience and Technology Division Report, PR106. Suva, 74 p.

Lichter, M; Vafeidis, A.T.; Nicholls, R.J., and Kaiser, G., 2011. Exploring Data-Related Uncertainties in Analyses of Land Area and Population in the "Low-Elevation Coastal Zone" (LECZ). *Journal of Coastal Research*, 27: 757–768.

McOwen, C.J.; Weatherdon, L.V.; Van Bochove, J.W.; Sullivan, E.; ... and Fletcher, S., 2017. A global map of saltmarshes. *Biodiversity data journal*, 5, e11764.

Neumann, B.; Vafeidis, A.T.; Zimmermann, J., and Nicholls, R.J., 2015. Future Coastal Population Growth and Exposure to Sea-Level Rise and Coastal Flooding - A Global Assessment. *PlosOne* 10(3): e0118571.

Sanderman, J.; Hengl, T.; Fiske, G.; Solvik, K.; ... and Duncan, C., 2018. A global map of mangrove forest soil carbon at 30 m spatial resolution. *Environmental Research Letters*, 13(5), 055002.

Sierra-Correa, P.C., and Kintz, J.R.C., 2015. Ecosystem-based adaptation for improving coastal planning for sea-level rise: A systematic review for mangrove coasts. *Marine Policy*, 51, 385-393.

Stumpf, R.P.; Holderied, K., and Sinclair, M., 2003. Determination of water depth with high-resolution satellite imagery over variable bottom types. *Limnology and Oceanography*, 48(1part2), 547-556.

Worliczek, E., 2013. La vision de l'espace littoral sur l'île Wallis et l'atoll Rangiroa dans le contexte du changement climatique (Doctoral dissertation, Nouvelle Calédonie).